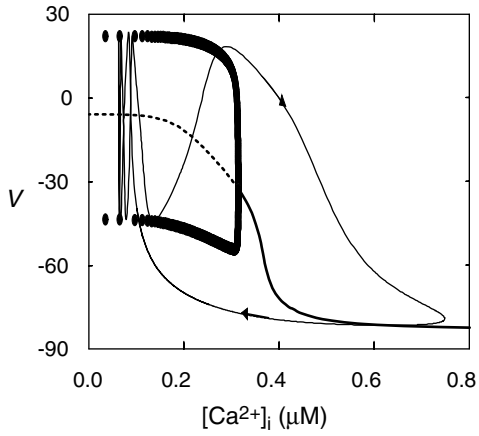

Figure 5.17 Full gonadotroph model: bifurcation diagram for the *dimensional* form of the fast subsystem (plasma membrane oscillator) with superimposed trajectory from Figure 5.16.

each voltage spike compensates the loss of Ca^{2+} to the extracellular medium and is thus key in preventing the store from depleting (see Li et al. (1997) for details of such interactions).

In Figure 5.17 the *dimensional* bifurcation diagram of the fast subsystem (the PM oscillator) with respect to $[Ca^{2+}]_i$ is shown with the trajectory of the bursting oscillations in the top panel of Figure 5.16 superimposed. Notice that the PM voltage V follows the diagram well during the spiking phase, when $[Ca^{2+}]_i$ changes slowly. But during the $[Ca^{2+}]_i$ spike, which is fast, the trajectory does not follow the diagram closely.

5.4 The Pancreatic Beta Cell

Pancreatic β-cells secrete insulin, the hormone that maintains blood plasma glucose within narrow limits in the face of variable food ingestion and physical activity patterns. Insulin allows muscle to take up glucose for immediate energy, causes the liver to store glucose as glycogen for medium-term energy storage, and signals fat cells to use glucose for fat deposition for long-term energy storage. Diabetes is a disease in which glucose is chronically elevated, leading to blindness, kidney failure, limb amputation, cardiovascular disease, and death. Type I ("juvenile") diabetes is the result of an absolute lack of insulin following auto-immune destruction of the β-cells. Type II ("adult onset") diabetes, the more common variety, involves a relative lack of insulin, usually as a result of two defects: insulin resistance (higher than normal concentrations of insulin are required for glucose processing) and failure of the β-cells to produce enough insulin to compensate. The rising tide of diabetes in the industrialized nations suggests that Type II diabetes is a maladaptive response to a toxically energy-rich food environment, with genes governing the susceptibility of individuals. For an entree into the vast literature on glucose homeostasis and diabetes see Porte, Jr. (1990) and Taylor (1999).

A number of aspects of this system have been modeled, including the kinetics of insulin secretion (Grodsky 1972), the etiology of diabetes as β-cells fail to compensate (Topp et al. 2000), insulin action (Quon and Campfield 1991a; Quon and Campfield 1991b), and whole-body plasma insulin oscillations (see Keener and Sneyd (1998) Chapter 19).

Here we limit our attention to the electrical activity and Ca^{2+} oscillations used by the β-cell to regulate insulin secretion. In terms of cell physiology, the β-cell closely resembles the pituitary gonadotroph. Both are endocrine cells in which secretion is controlled by $[Ca^{2+}]_i$, which is in turn regulated to a large degree by bursting, and they share many mechanistic elements such as K(Ca) channels and IP_3 receptors. However, there are important and interesting differences from that point on. Bursting in β-cells is primarily driven by the plasma membrane oscillator, though the ER probably plays a significant role at least in modulating the burst mechanism.

These characteristics are shared with many neurons, and β-cells provided an early paradigm for modeling of bursting. See Rinzel and Ermentrout (1998) or Keener and Sneyd (1998).

The models discussed in this section are complementary to the Keizer–Maki model in Chapter 4. The latter considers insulin oscillations but does not explicitly treat the Ca^{2+} influx that leads to insulin secretion. Here we treat Ca^{2+} influx in detail, but assume that secretion increases with mean $[Ca^{2+}]_i$.

We will focus on membrane-potential-driven $[Ca^{2+}]_i$ oscillations, though β-cells have occasionally been observed to exhibit oscillations driven by the ER, similar to those in gonadotrophs. Ironically, the Keizer–DeYoung model for the IP_3 receptor was originally developed to explain this marginal phenomenon in β-cells, and was then ready at hand for application to gonadotrophs.

One indication of the differences between β-cell and gonadotroph bursting is apparent in Figure 5.18. This simultaneous recording of membrane potential and $[Ca^{2+}]_i$ oscillations shows that $[Ca^{2+}]_i$ is high during the depolarized spiking phase of the bursts, rather than during the hyperpolarized silent phase. Compare with Figure 5.11.

An important aspect of β-cell function that we will also have to neglect in this chapter is the organization of the cells into electrically coupled populations, called the islets of Langerhans. Here we take advantage of the observation that the cells in an islet are synchronized. That is why the voltage of the single peripheral cell shown in Figure 5.18B is in register with the $[Ca^{2+}]_i$ signal (Figure 5.18A), which comes from many cells in the islet. This allows us to study a simple single-cell model, which can be taken as representative of the whole islet. More subtle effects of electrical coupling will be discussed in Chapter 6. See also Sherman (1997).

5.4.1 Chay–Keizer Model

The model we use to illustrate β-cell bursting is based loosely on the model of Sherman et al. (1988), recast in Morris–Lecar form. Bursting occurs in response to glucose, so no applied current is needed. Morris–Lecar by itself can account for the spiking during the

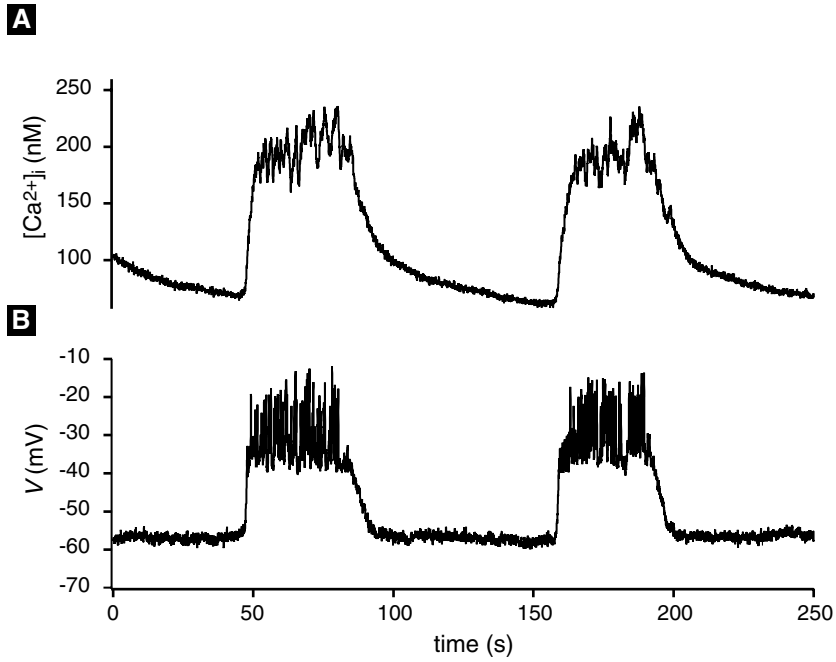

Figure 5.18 Simultaneous recording of membrane potential bursts and Ca^{2+} oscillations from a pancreatic islet of Langerhans. V recorded by perforated patch on a peripheral β-cell. $[Ca^{2+}]_i$ recorded from whole islet using fura-2. Data provided by Drs. Les Satin and Min Zhang, Virginia Commonwealth University.

active phase of a burst. In order to obtain cycling between bursting and silent phases, we need to add a slow negative–feedback current. The first hypothesis, proposed by Atwater, Rojas, and colleagues (Atwater et al. 1980) and made into a mathematical model by Chay and Keizer (1983), was that bursting was mediated by a K(Ca) current. The idea was that $[Ca^{2+}]_i$ would build up slowly during the spiking phase until the inhibitory effect of the increased K^+ current reached a sufficiently high level to terminate the spiking. The K(Ca) current is represented as

$$I_{K(Ca)} = g_{K(Ca)} \frac{[Ca^{2+}]_i}{K_{K(Ca)} + [Ca^{2+}]_i} (V - V_K), \tag{5.60}$$

and the modified Morris–Lecar equations, supplemented by a slow equation for $[Ca^{2+}]_i$, are

$$C_m \frac{dV}{dt} = -I_{Ca} - I_K - I_L - I_{K(Ca)}, \tag{5.61}$$

$$\frac{dw}{dt} = \phi \frac{w_\infty - w}{\tau}, \tag{5.62}$$

$$\frac{d[Ca^{2+}]_i}{dt} = f_i(-\alpha I_{Ca} - v_{LPM}[Ca^{2+}]_i). \tag{5.63}$$

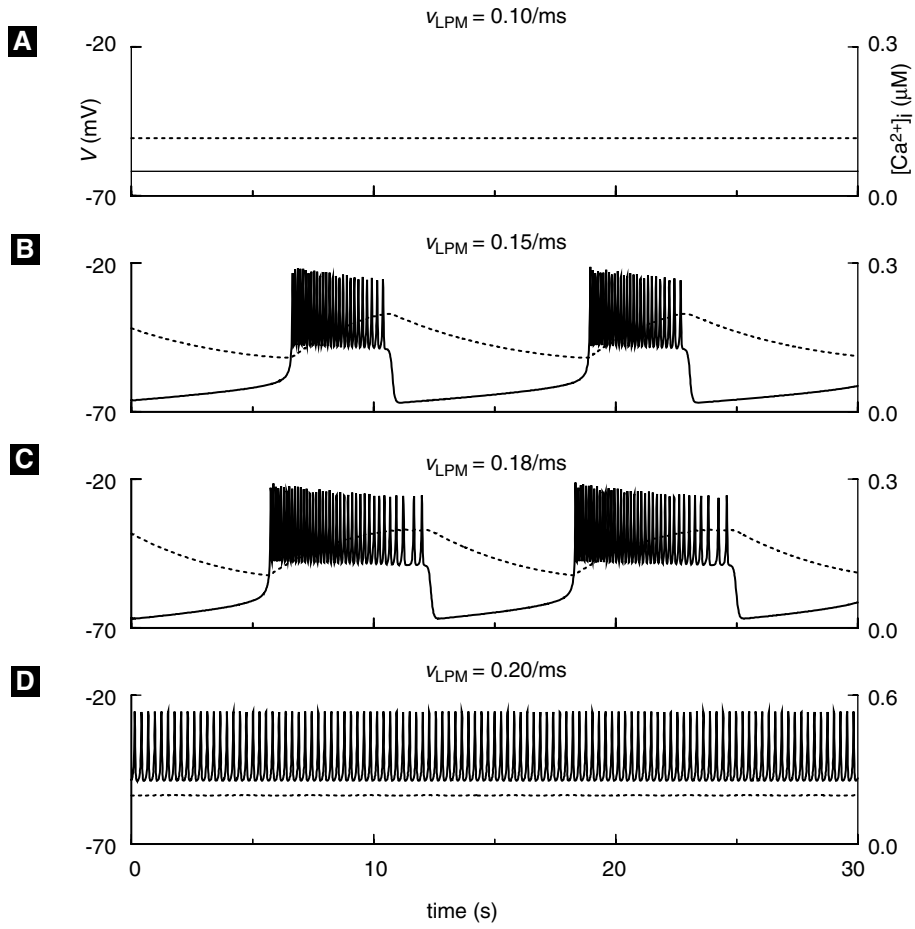

Figure 5.19 Bursting and glucose sensing of the Chay–Keizer model, (5.61)–(5.63). Parameters: $C_m = 5300$ fF, $g_{Ca} = 1000$ pS, $V_{Ca} = 25$ mV, $g_K = 2700$ pS, $V_K = -75$ mV, $I_{app} = 0$, $v_1 = -20$ mV, $v_2 = 24$, $v_3 = -16$ mV, $v_4 = 11.2$ mV, $\phi = 0.035$/ms, $g_L = 150$ pS, $V_L = -75$ mV, $g_{K(Ca)} = 2000$ pS, $K_{K(Ca)} = 5$ μM, $f = 0.001$, $\alpha = 4.5 \times 10^{-6}$ μM/(fA· ms), and v_{LPM} as indicated.

Here f_i is the fraction of free $[Ca^{2+}]_i$, and $\alpha = 10^3/(2F\overline{V}_i)$ converts current in fA to μM/ms (cf. (5.27)). The term $v_{LPM}[Ca^{2+}]_i$ is a linearized representation of the PMCA. We will refer to this model as "Chay–Keizer" for brevity because it is based on the same mechanisms, but see (Chay and Keizer 1983) for details of the original. For nondimensionalization and applications, see (Pernarowski et al. 1992).

Numerical results are shown in Figure 5.19. Focusing first on panels B and C, we see that bursting can occur without participation of the ER; all that is needed is a slow negative–feedback process, here supplied by $[Ca^{2+}]_i$.

Because $[Ca^{2+}]_i$ varies very slowly, we can analyze the dynamics by decomposing the system into simpler components, one fast and one slow. The first step is to view

$[Ca^{2+}]_i$ as a parameter that controls the behavior of the fast subsystem, consisting of V and n. In analogy to Figure 5.9, we construct the bifurcation diagram of the fast subsystem with respect to $[Ca^{2+}]_i$. Figure 5.20A shows the resulting three-branched Z-shaped curve (Z-curve) of steady states. The Z-curve is actually the projection into the V-$[Ca^{2+}]_i$ plane of the three-dimensional curve on which V and n are at steady state. When $[Ca^{2+}]_i$ is high, $g_{K(Ca)}$ is large, and the system goes to the lower branch of low-voltage steady states. When $[Ca^{2+}]_i$ is low, $g_{K(Ca)}$ is small, and V rises above the threshold for activation of the voltage-dependent Ca^{2+} and K^+ currents, generating the depolarized upper branch. For intermediate values of $[Ca^{2+}]_i$ there are three steady states. The new steady states are born via saddle-node bifurcations, with the saddle points making up the middle branch of the Z-curve.

The fast subsystem consists of two variables, not just one as was the case in Figure 5.9, so it can itself undergo oscillations, even with $[Ca^{2+}]_i$ fixed. These oscillations arise via a Hopf bifurcation on the upper branch and correspond to the fast spikes during a burst. For intermediate values of $[Ca^{2+}]_i$, the system is bistable: It can either be at rest on the lower branch of the Z-curve or oscillate on the upper branch. Bursting is a repetitive alternation between these two states. In order for this to occur, $[Ca^{2+}]_i$ must have appropriate slow dynamics, such that it increases when V is high and decreases when V is low. We can interpret this geometrically by ignoring n and viewing the V-$[Ca^{2+}]_i$ bifurcation diagram as a V-$[Ca^{2+}]_i$ phase plane (Figure 5.20B). The Z-curve serves as a nullcline for V, and we add a nullcline for $[Ca^{2+}]_i$, which increases when the phase point is above the $[Ca^{2+}]_i$ nullcline and decreases when the point is below the nullcline. Thus, in order for $[Ca^{2+}]_i$ to rise during the active phase of each burst and fall during the silent phase, the $[Ca^{2+}]_i$-nullcline must intersect the middle branch of the Z-curve. If instead the $[Ca^{2+}]_i$-nullcline intersects the lower branch, the cell will remain silent. If the $[Ca^{2+}]_i$-nullcline intersects the spiking branch, the cell can fire continuously; the influx of $[Ca^{2+}]_i$ during each spike exactly balances the removal.

To understand this analysis in depth, it is helpful to construct the phase planes corresponding to different values of $[Ca^{2+}]_i$ (Exercise 13). Of particular interest is the key role of the homoclinic orbit (labeled HC in Figure 5.20A) in terminating the active phase of each burst. See also Sherman (1997) or Rinzel and Ermentrout (1998).

Returning to Figure 5.19, the sequence of panels illustrates how β-cells modify their electrical activity according to the level of glucose. As glucose concentration increases, the rate of the PMCA is here hypothesized to increase as well. For low glucose (low pump rate), the cell is electrically silent (top panel). For glucose above a threshold concentration, bursting appears (second panel). Further increases in glucose result in longer active spiking phases, or plateaus, and shorter silent phases (third panel). Finally, for very high glucose, the cell remains permanently in the active phase, spiking continuously. Comparing these stattements to the bifurcation analysis (Figure 5.20), we find that those about glucose and pump rate are equivalent to statements about how the $[Ca^{2+}]_i$-nullcline intersects the Z-curve. An alternative scenario for glucose sensing is described in Exercise 10.

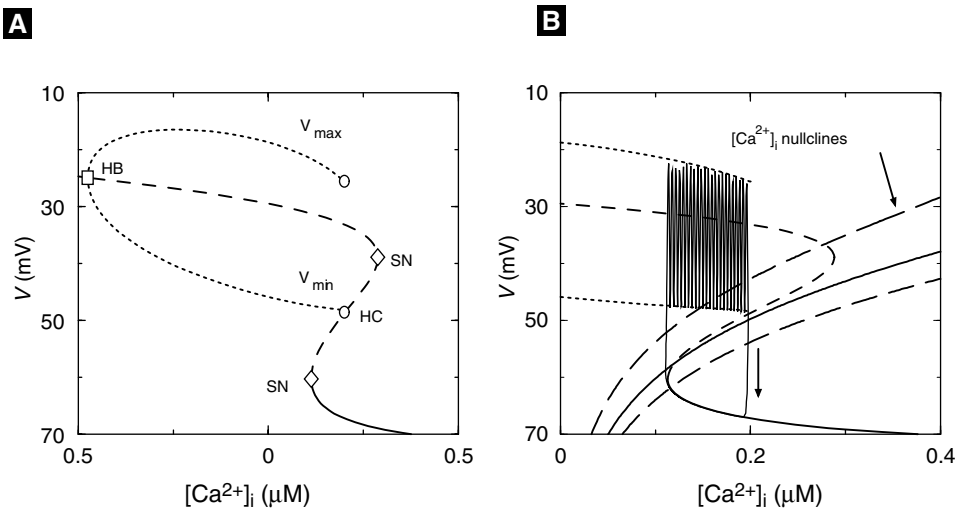

Figure 5.20 (A) Bifurcation diagram of Chay–Keizer fast equations (5.61)–(5.62) using $[Ca^{2+}]_i$ as a parameter. Hopf bifurcation (HB – square); saddle-nodes (SN – diamonds); homoclinic orbit (HC – circles). (B) Projection of V-$[Ca^{2+}]_i$ trajectory for $v_{LPM} = 0.13\ ms^{-1}$ onto the bifurcation diagram. Vertical arrow next to trajectory indicates direction of increasing time. Nullclines for $[Ca^{2+}]_i$ are shown for three cases: $v_{LPM} = 0.10$ (bottom), $v_{LPM} = 0.13$ (middle), and $v_{LPM} = 0.20$ (top). The corresponding solutions are silent, bursting, and continuously spiking, respectively. Compare with Figure 5.19.

5.4.2 Chay–Keizer with an ER

The ER is significant in β-cells for two reasons. One is that an important potentiator of insulin secretion, acetylcholine (ACh), works by promoting production of IP_3 and dumping the stores, similar to GnRH in gonadotrophs. This has been modeled in Bertram et al. (1995) and Chay (1997).

The second reason is that the ER strongly influences the kinetics of $[Ca^{2+}]_i$, and hence all $[Ca^{2+}]_i$-dependent processes. Here we consider only the latter aspect, showing that even a passive ER, which does not actively dump Ca^{2+}, can have profound effects on bursting. To do this we append an equation for $[Ca^{2+}]_{ER}$ to the Chay–Keizer model and add appropriate flux terms, a passive conductance and a linearized version of the SERCA pump (with leading constant v_{LSP}), to the $[Ca^{2+}]_i$ equation:

$$C_m \frac{dV}{dt} = -I_{Ca} - I_K - I_{K(ATP)} - I_{K(Ca)}, \tag{5.64}$$

$$\frac{dw}{dt} = \phi \frac{w_\infty - w}{\tau}, \tag{5.65}$$

$$\frac{d[Ca^{2+}]_i}{dt} = f_i(-\alpha I_{Ca} - v_{LPM}[Ca^{2+}]_i)$$

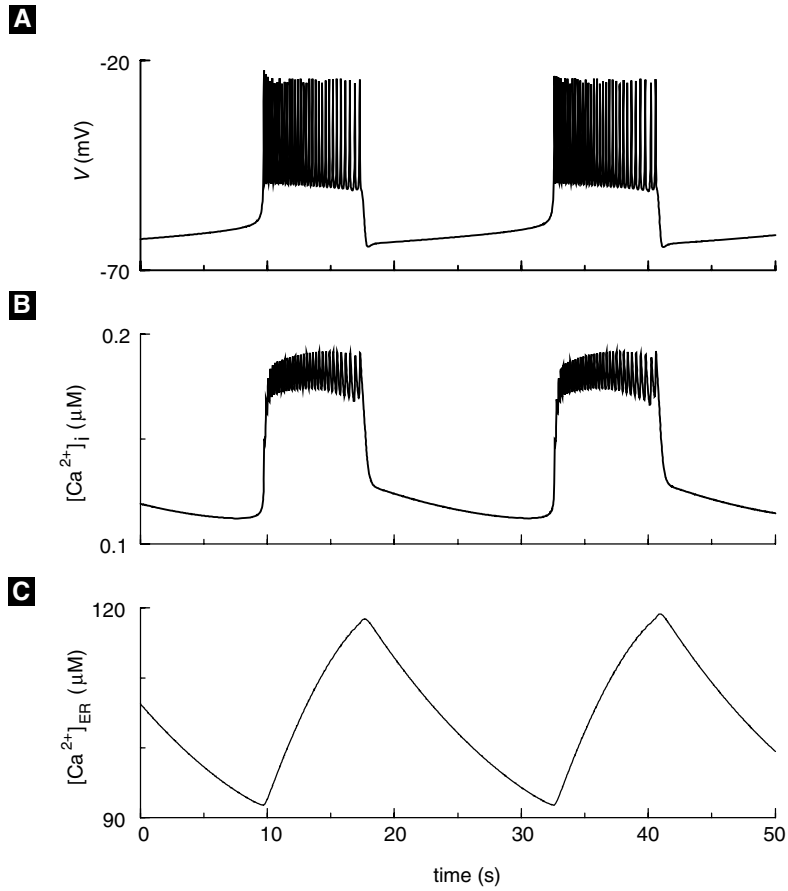

Figure 5.21 Bursting in the Chay–Keizer model with ER, (5.64)–(5.67). Parameters as in Figure 5.19, except $f_i = 0.01$, with the following parameters added for the ER: $P_{IP3R} = 0.0008$/ms, $\lambda = 2$, $\sigma = 0.032$, $v_{LSP} = 0.6$/ms.

$$+ \frac{f_i}{\lambda_{ER}} \left(P_{IP3R}([Ca^{2+}]_{ER} - [Ca^{2+}]_i) - v_{LSP}\,[Ca^{2+}]_i \right), \tag{5.66}$$

$$\frac{d[Ca^{2+}]_{ER}}{dt} = \frac{f_i}{\sigma\lambda_{ER}} \left(-P_{IP3R}([Ca^{2+}]_{ER} - [Ca^{2+}]_i) + v_{LSP}\,[Ca^{2+}]_i \right). \tag{5.67}$$

Compare these equations with (5.23) and (5.24). Although $[Ca^{2+}]_{ER}$ does not directly affect the plasma membrane, it has indirect effects through $I_{K(Ca)}$. This model is essentially equivalent to Theresa Chay's last β-cell model (Chay 1997).

Bursting with this model is shown in Figure 5.21. Here f_i has been increased to 0.01, which means that in the absence of the ER only very fast bursting can occur (see Exercise 12). In this case, bursting with periods of 10–60 seconds, as typically observed in islets, depends on slow kinetics supplied by the ER. Note that $[Ca^{2+}]_{ER}$ rises and

falls slowly the way $[Ca^{2+}]_i$ does in the original Chay–Keizer model (cf. Figure 5.19). In contrast, $[Ca^{2+}]_i$ shows two distinct time scales, fast jumps at the beginning and end of each burst, a slowly rising plateau during the active phase, and a slow tail during the silent phase. The fast jumps reflect the intrinsic kinetics of $[Ca^{2+}]_i$, while the slow portions reflect slow uptake and release of Ca^{2+} by the ER. This complex time course matches the characteristics of $[Ca^{2+}]_i$ seen in experiments (see Figure 5.18 and also Valdeolmillos et al. (1989)) better than Chay–Keizer (Figure 5.19). It also demonstrates that it is possible for slow negative feedback to operate through the K(Ca) channel, or some other Ca^{2+}-sensitive channel, even though $[Ca^{2+}]_i$ does not itself appear to be slow.

The examples discussed here represent only the tip of the iceberg of the β-cell field. The precise contributions of the mechanisms we have treated, K(Ca) channels, $g_{K(ATP)}$ channels, and the ER, as well as some that we have not treated, such as inactivation of Ca^{2+} channels, are not settled. However, it seems likely that complex interactions of all of these will be necessary to explain the diverse phenomena observed. The mechanisms of other important regulators of cell electrical activity and $[Ca^{2+}]_i$, such as cAMP and epinephrine, remain to be elucidated. Nonetheless, the basic mechanisms and concepts presented here should prepare the reader sufficiently to explore the exercises and the literature on his or her own.

Suggestions for Further Reading

- *Ryanodine receptor adaptation and Ca^{2+}-induced Ca^{2+} release-dependent Ca^{2+} oscillations*, Joel Keizer and Leslie Levine. This paper is the original source for the Keizer–Levine model (Keizer and Levine 1996).
- *Ca^{2+} excitability of the ER membrane: an explanation for IP_3-induced* Ca^{2+} *oscillations*,Yue Xian Li, Joel Keizer, Stanko S. Stojilković, and John Rinzel. A review of how the gonadotroph model described here was developed, with some equations and discussion of scaling and references to the physiolgical literature (Li et al. 1995b).
- *$InsP_3$-induced Ca^{2+} excitability of the endoplasmic reticulum*, Joel Keizer, Yue Xian Li, Stanko Stojilković, and John Rinzel. Another review of the gonadotroph, but in words and pictures. This review contains many references to the physiological literature (Keizer et al. 1995).
- *Contributions of modeling to understanding stimulus-secretion coupling in pancreatic β-cells*, Arthur Sherman. A review of β-cell modeling oriented toward biologists (Sherman 1996).
- *Calcium and membrane potential oscillations in pancreatic β-cells*, Arthur Sherman. A mathematical tutorial centered on β-cell models with some connections to general modeling of bursting. Covers phase plane and bifurcation analysis (Sherman 1997).

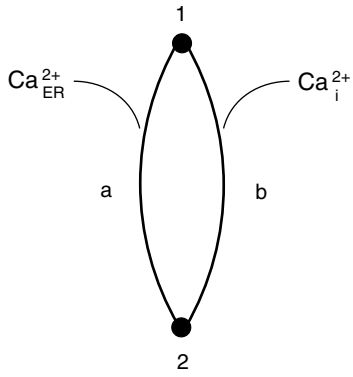

Figure 5.22 Kinetic diagram for ER leak.

5.5 EXERCISES

1. Generalize (5.13) to the case of (a) two and (b) arbitrarily many buffers.

2. The expression for ER leak (5.26) can be derived from a symmetric cycle model (Fig. 5.22) representing a pore that can exist in either an unbound state (1) or a bound state (2) and bind Ca^{2+} on either the ER or the cytosolic side. A cycle from 1 to 2, binding Ca^{2+} on the ER side, and back to 1, releasing Ca^{2+} on the cytosolic side transports 1 ion from the ER to the cytosol. Assume symmetry, that is, the rates of binding $[Ca^{2+}]_i$ and $[Ca^{2+}]_{ER}$ are equal, $k_{12}^{a*} = k_{12}^{b*} = k_{12}^{*}$, and the rates of releasing $[Ca^{2+}]_i$ and $[Ca^{2+}]_{ER}$ are equal, $k_{21}^{a} = k_{21}^{b} = k_{21}$, and use the diagrammatic method of Chapter 3 to show that

$$J^{ss} = J_{21}^{ssb} = \frac{k_{12}^{*}}{2}([Ca^{2+}]_{ER} - [Ca^{2+}]_i) \tag{5.68}$$

in an appropriate limit. (The quantity $[Ca^{2+}]_{ER} - [Ca^{2+}]_i$ is called the thermodynamic driving force.)

3. (a) Write down the mass action equations corresponding to the Keizer–Levine kinetic diagram in Figure 5.5 and calculate the steady-state fraction of open channels (those in states O1 or O2) as a function of Ca^{2+}. Compare to the plateau curve in Figure 5.6.

   (b) Approximate the peak open fraction following a step of Ca^{2+} from rest by assuming that C2 does not change over short times. Compare to the peak curve in Figure 5.6.

   (c) Derive the quasi-steady-state approximation (5.28)–(5.31). Hint: Combine the result in (b) with a differential equation for $w = 1 - P_{C2}$ assuming that transitions among O1, O2, and C1 are in rapid equilibrium. Simulate the two-pulse experiment of Figure 5.6 and verify that the quasi-steady-state approximation retains the feature of adaptation.

   (d) Draw the reduced diagram. What are the expressions for the reduced rate constants?

4. (a) By calculating the Jacobian of the closed-cell Keizer–Levine model (Section 5.2.2), show that for oscillations to arise via a Hopf bifurcation, it is necessary for the w and $[Ca^{2+}]_i$ nullclines to intersect with negative slope and with the w nullcline steeper.

   (b) Using the result of (a), find parameter values for which there are stable oscillations graphically, by plotting the nullclines, or analytically, by solving the w and $[Ca^{2+}]_i$ equations in terms of w. Hint: One way is to play with the affinity of the SERCA pump.

(c) (optional) Construct the bifurcation diagram for the modified system and plot the period vs. $[Ca^{2+}]_T$. Correlate changes in the period with changes in the phase plane, particularly the invariant sets of the saddle point.

(d) Find the s-curve analytically by isolating $[Ca^{2+}]_T$.

5. (a) Plot period vs. j_{IN} for the reduced open-cell Keizer–Levine model (Section 5.2.3).

(b) Compare the range of j_{IN} for which there are oscillations predicted by the phase plane to those calculated in the bifurcation diagram. Using the phase plane in Figure 5.9, explain the variation in period.

(c) (optional) Compare the variation in period with that in the Chay–Keizer β-cell model when $g_{K(Ca)}$ is varied (Figure 5.19, Figure 5.20).

6. (a) Solve the Keizer–Levine open-cell system and find values of j_{IN} that support oscillations. Compare the extent of store dumping with the closed–cell oscillations (Exercise 4). Plot the fluxes across the plasma membrane and ER through the cycle.

(b) Investigate the effect of increasing k_c^- and explain what this implies about the reduced open–cell model with $w = w_\infty$.

(c) (optional) Construct the bifurcation diagram with j_{IN} as a parameter and compare to Figure 5.10.

7. (a) Create a table of nondimensional parameter values from the dimensional parameters corresponding to Figure 5.12 for the closed-cell gonadotroph model (Section 5.3.1).

(b) Implement and solve both the dimensional and nondimensional forms of closed-cell gonadotroph model (Section 5.3.1) at $[IP_3] = 1.0$ and compare the results.

(c) For the same parameter values as in Figure 5.13B (dotted curve), show that oscillations can occur by either decreasing the value of K_a (Ca^{2+} sensitivity of the activation gate) or increasing the value of $[Ca^{2+}]_T$.

8. (a) Write out the dimensional version of the open–cell gonadotroph model (5.48)–(5.50). Start by adding j_{IN} and j_{PMCA} (cf. (5.37)) to (5.40) and writing an equation for $[Ca^{2+}]_{ER}$. Then nondimensionalize to obtain (5.48)–(5.50). Hint: Express the fluxes in terms of flux per unit area. For example, define $\mathcal{V}_{PMCA} = V_{PMCA}/A_{PM}$, where A_{PM} is the plasma membrane area.

(b) Simulate the open-cell gonadotroph model (5.48)–(5.52) with the same parameter values as in Figure 5.14.

(c) Show that at small, positive, and constant values of $\hat{j}_{in}$, intermittent intermittent or waxing-and-waning type of "bursting" can ooccur in the open-cell gonadotroph model.

(d) Explain this phenomenon by using a bifurcation diagram similar to that in Figure 5.15.

9. Slow, influx-driven Ca^{2+} oscillations observed in bullfrog sympathetic neurons (see Figure 5.8) can also occur in cells that express only IP_3R channels. This can be demonstrated by the open-cell gonadotroph model (Section 5.3.2) described by (5.48)–(5.52).

(a) Let $\epsilon = 0$. Plot the bifurcation diagram of the resulting 2-variable closed-cell model as a function of $\hat{c}_T$ at decreasing values of $\hat{k}_S$ while keeping other parameter values

identical to those given in Figure 5.15. Determine a value of $\hat{k}_S$ that yields an "S"-shaped, bistable diagram similar to that in Figure 5.7B. Then, simulate the whole model to generate slow oscillations similar to those in Figure 5.8.

(b) For the same parameter values used in (a), show that you get almost identical slow oscillations by eliminating the h equation and replacing h with $h_\infty = 1/(1+\hat{c})$ in the other two equations. Explain why.

10. One criticism of the glucose-sensing in the Chay–Keizer model (Figure 5.19) is that even though the cell visually appears to be more active electrically in higher glucose, mean $[Ca^{2+}]_i$ does not increase much. An alternative model that addresses this problem uses the K(ATP) channel, a K^+ channel that is inhibited by ATP and activated by ADP. It is thus a natural link between glucose metabolism and membrane potential.

(a) Starting with Chay–Keizer, set $g_L = 0$ and add the current

$$I_{K(ATP)} = g_{K(ATP)}(V - V_K) \tag{5.69}$$

to the V-equation. Calculate the solution for $g_{K(ATP)} = 160$, 150, 135, and 130 and describe the changes in plateau fraction and $[Ca^{2+}]_i$ compared to Figure 5.19.

(b) Explain your results in terms of the biophysics of $g_{K(ATP)}$.

(c) Derive a formula for the Z-curve by solving for $[Ca^{2+}]_i$. Describe algebraically and geometrically the effect of varying $g_{K(ATP)}$.

(d) Using the result of (c) or just constructing bifurcation diagrams for different values of $g_{K(ATP)}$, explain geometrically the effects of $g_{K(ATP)}$.

11. Keizer and Magnus (1989) proposed that $g_{K(ATP)}$ played not simply a modulatory role in bursting, but could itself provide slow negative feedback. They hypothesized that a rise in $[Ca^{2+}]_i$ would lead to mitochondrial uptake of Ca^{2+} and dissipate the mitochondrial membrane potential that provides the energy for ATP synthesis. Thus, as $[Ca^{2+}]_i$ rises, ATP falls and ADP rises.

(a) Show, assuming that ATP and ADP compete for the same binding site, that

$$g_{K(ATP)} = \bar{g}_{K(ATP)} \frac{1 + [ADP]/K_1}{1 + [ADP]/K_1 + [ATP]/K_2}. \tag{5.70}$$

(b) Add the following simplified equation for mitochondrial dynamics to Chay–Keizer (with $I_{K(ATP)}$ as in (5.69) included in the V equation):

$$\frac{d[ADP]}{dt} = v_{MITO}\left([ATP] - [ADP]\exp\left(R\left(1 - \frac{[Ca^{2+}]_i}{R_1}\right)\right)\right). \tag{5.71}$$

Assume that

$$[ADP] + [ATP] = 1 \text{ mM} \tag{5.72}$$

and simulate the solution to get bursting using the parameter values from Figure 5.19 except that $K_c = 0.15$/ms, $g_{K(Ca)} = 0$ pS, $g_L = 0$ pS, $f_i = 0.01$, and add the following new parameters for metabolic feedback: $\bar{g}_{K(ATP)} = 6000$ pS, $K_1 = 0.45$ mM, $K_2 = 0.012$ mM, $R = 0.9$, $R_1 = 0.35$ mM, $v_{MITO} = 5.0 \times 10^{-5}$/ms.

(c) Show that the parameter R can function as a glucose sensor. Should R increase or decrease with glucose?

12. (a) Remove the ER from the Chay–Keizer model with ER and solve, retaining all other parameters from Figure 5.21. What is the burst period?

(b) Add the ER back, and construct the bifurcation diagram of the model (5.64)–(5.67) using $[Ca^{2+}]_{ER}$ as the bifurcation parameter. Explain how $[Ca^{2+}]_{ER}$ can act as a slow variable even though it does not appear in the V equation. Use the diagram to explain how varying σ (5.67) changes the burst period.

(c) Make another bifurcation diagram for this model using $[Ca^{2+}]_i$ as the bifurcation parameter, with $[Ca^{2+}]_{ER}$ held constant. Overlay the $[Ca^{2+}]_i$ nullcline. How does the diagram change as $[Ca^{2+}]_{ER}$ is varied?

(d) Increase P_{IP3R} (5.66) to 0.008/ ms. Use the two bifurcation diagrams from (b) and (c) to analyze the effect of P_{IP3R} on burst frequency. Compare with (Chay 1997).

(e) (optional) Restore P_{IP3R} to 0.0008/ms and increase λ (5.66) to 800. Use the bifurcation diagram from (c) to explain why the burst frequency increases.

13. Construct phase planes of the Chay–Keizer fast subsystem (5.61), (5.62) with $[Ca^{2+}]_i$ as a parameter and correlate the various patterns with the bifurcation diagram Figure 5.20. Look for stable and unstable nodes, saddle points, and periodic orbits. Choose values in each of the regimes defined by the bifurcation diagram:

- just to the left and just to the right of the Hopf bifurcation
- just to the left and just to the right of the point labeled SN
- just to the left and just to the right of the point labeled HC (for homoclinic orbit).

Explain why the period increases sharply as the HC is approached from the left. Explain why the period solution disappears at HC. It will help to draw the stable and unstable manifolds of the saddle point.